International Journal of Remote Sensing
Vol. 31, No. 16, 20 August 2010, 4295–4318

Taylor & Francis
Taylor & Francis Group

Global patterns in daytime cloud properties derived from GOME backscatter UV-VIS measurements

D. G. LOYOLA R.*†, W. THOMAS‡, R. SPURR§ and B. MAYER¶|
†Deutsches Zentrum für Luft- und Raumfahrt (DLR), Institut für Methodik der Fernerkundung (IMF), Oberpfaffenhofen, D-82234 Wessling, Germany
‡Deutscher Wetterdienst (DWD), Hohenpeißenberg Meteorological Observatory, D-82383 Hohenpeißenberg, Germany
§RT Solutions, Inc., 9 Channing Street, Cambridge, MA 02138, USA
¶Deutsches Zentrum für Luft- und Raumfahrt (DLR), Institut für Physik der Atmospähre (IPA), Oberpfaffenhofen, D-82234 Wessling, Germany
|Lehrstuhl für Experimentelle Meteorologie, Ludwig-Maximilians-Universität, Theresienstrasse 37, 80333 München, Germany

(*Received 24 October 2008; in final form 26 December 2008*)

In this paper, we present an overview of the cloud property data set derived from 8 years of reflected solar ultraviolet-visible (UV-VIS) measurements taken by the global ozone monitoring experiment (GOME) instrument from April 1996 to June 2003. We consider four such properties: cloud amount, cloud-top pressure, cloud optical thickness and cloud type. Cloud amounts are generated from GOME broad-band polarization data using data fusion techniques, while cloud-top height (pressure) and cloud-top albedo are retrieved from GOME backscatter measurements in the oxygen (O_2) *A*-band via neural network inversion of simulated reflectances. Cloud optical thickness is derived as an additional parameter from the cloud-top albedo and radiative transfer model simulations, and cloud type is determined from the cloud-top pressure and optical thickness. We analyse global and seasonal patterns for these properties, looking at monthly means, standard deviations and the 8-year average values. We compare GOME results with the longer-period multisatellite international satellite cloud climatology project (ISCCP) D-series cloud climatology. The overall good agreement demonstrates that GOME provides accurate and complementary cloud information. Differences in cloud amount, cloud-top height and optical thickness values are due primarily to contrasting measurement strategies (GOME measures daytime-only UV-VIS backscatter, ISCCP is based on several day and night infrared satellite observations). We look forward to the extension of this UV-VIS cloud parameter series with the advent of more recent backscatter atmospheric composition instruments such as the scanning imaging absorption spectrometer for atmospheric cartography (SCIAMACHY) on-board the environmental satellite (ENVISAT) and the GOME-2 series on the MetOp platforms.

1. Introduction

The generation of long-term, homogeneous data series of satellite-based cloud properties started in the early eighties with the international satellite cloud climatology project

*Corresponding author. Email: diego.loyola@dlr.de

International Journal of Remote Sensing
ISSN 0143-1161 print/ISSN 1366-5901 online © 2010 Taylor & Francis
http://www.tandf.co.uk/journals
DOI: 10.1080/01431160903246741

(ISCCP) (Schiffer and Rossow 1983); see also Rossow and Schiffer (1999) and references therein. Other data sets are, for example, the globally available Advanced Very High Resolution Radiometer (AVHRR) Pathfinder Atmosphere (PATMOS) data set (Jacobowitz *et al.* 2003), the Swedish Meteorological and Hydrological Institute (SMHI) Cloud Analysis model using Digital AVHRR data (SCANDIA) cloud climatology (Karlsson 2003) over Scandinavia and the European Cloud Climatology (Meerkötter *et al.* 2004), all of which were derived from AVHRR observations. Wylie *et al.* (2005) provide a 20-year time series of cloud parameters derived from high resolution infrared radiation sounder (HIRS) observations in the infrared spectral range. Such data series are needed to detect possible weaknesses of climate simulations (Karlsson *et al.* 2008). A prerequisite for using satellite-based data records for trend studies and the detection of climate change is the generation of homogeneous and stable data sets from recent, current and future satellite sensors (Ohring *et al.* 2005). For example, Lindström *et al.* (2006) showed that the AVHRR-based Pathfinder data set (Smith *et al.* 1997) is affected by the annual orbital drift of the National Oceanic & Atmospheric Administration (NOAA) spacecrafts, i.e. the corresponding variation of the solar zenith angle, and existing time series must therefore be handled with care. More recently, Evan *et al.* (2007) found no obvious trend in one of the longest existing cloud parameter time series – the ISCCP data set. As discussed by Evan *et al.* (2007), this is in contrast to conclusions drawn from previous studies; this shows the importance of performing a careful data analysis before reliable information about the climate system becomes available.

Space-borne trace gas measurements in the UV-VIS spectral range require precise knowledge of cloud properties and several recent studies therefore dealt with the retrieval of cloud properties from the global ozone monitoring experiment (GOME) measurements: Kuze and Chance (1994) provided a first algorithm approach to retrieve cloud fraction and cloud-top height from GOME measurements in the oxygen *A*- and *B*-bands that was the basis of the cloud parameter retrieval algorithm applied in previous versions of the operational GOME data processor system (Spurr *et al.* 2005). This work was refined and enhanced by Koelemeijer *et al.* (2001) and a first comparison of GOME cloud observations (effective cloud fraction, cloud-top pressure) with the ISCCP data set was presented in a study by Koelemeijer *et al.* (2002). The authors found reasonably good agreements for cloud fraction and cloud-top height for the two months analysed. Tuinder *et al.* (2004) compared cloud fraction results of several GOME cloud retrieval algorithms to synoptic surface observations, including a predecessor version of the algorithm used in this study (Loyola *et al.* 2007), which performed well. A combined algorithm for the determination of cloud fraction and cloud-top height was recently developed by Grzegorski *et al.* (2006). All these algorithms provide so called '*effective*' cloud parameters retrieved assuming a fixed cloud optical thickness (or cloud-top albedo/reflection). In contrast to these algorithms our approach does not have such a limitation, as the cloud-top albedo is also retrieved from the GOME measurements (see next section). Furthermore Kokhanovsky *et al.* (2003) developed a semi-empirical cloud properties retrieval algorithm for the scanning imaging absorption spectrometer for atmospheric cartography (SCIAMACHY) instrument on-board environmental satellite (ENVISAT). Specifically, cloud optical thickness, the liquid water path and the effective size of water droplets are retrieved by this algorithm for water clouds with large optical thickness. Finally, Diedenhoven *et al.* (2007) presented a method for the retrieval of GOME cloud parameters using simultaneous measurements in the UV and in the O_2 *A*-band.

The GOME data record started in 1995 although global measurements have been compromised since June 2003 due to a tape recorder failure on the European Remote Sensing (ERS-2) satellite. Reliable and accurate trace gas measurements from remote sensing instruments depend upon knowledge of the spatial distribution of clouds, the top height of clouds and the cloud-top albedo (Loyola *et al.* 2007). As shown by Balis *et al.* (2007), the accuracy of GOME observations is now in the same range as ground-based measurements. Additionally, the cloud information is very useful for analysing ozone dynamics observations (Chandra and Varotsos 1995).

In this paper, we present a detailed analysis of retrieved and derived GOME cloud parameters and we compare the GOME 8-year cloud property record with data from ISCCP.

2. Retrieval and derivation of GOME cloud properties

A detailed description of the GOME instrument can be found for example in Burrows *et al.* (1999), and in particular with respect to cloud property retrieval in the more recent work of Loyola *et al.* (2007). The latter paper has detailed descriptions of two cloud property algorithms applied to GOME backscatter measurements. These two algorithms, Optical Cloud Recognition Algorithm (OCRA) and Retrieval of Cloud Information using Neural Networks (ROCINN), retrieve the cloud fraction, and cloud-top height (pressure) and cloud-top albedo (optical thickness) from GOME observations, respectively. These algorithms are part of the operational GOME Data Processing system for trace gas total column retrievals (Van Roozendael *et al.* 2006). A brief summary of these algorithms is given in the following two subsections: section 2.3 summarizes the derivation of cloud optical thickness, and section 2.4 contains a note on the computation of cloud averages.

2.1 *Cloud amount retrieval*

The basic idea of OCRA is to break down each optical sensor measurement into two components: a cloud-free background and a residual contribution expressing the influence of clouds. The key component of the algorithm is a cloud-free composite reflectivity map that is corrected for atmospheric and topographic effects, and for illumination and viewing geometry. The composite has been generated from GOME observations and consists of a global set of the minimum reflectivities. Three such reflectivity maps have been generated from measurements made by the three broad-band GOME Polarization Measurement Devices (PMDs). One PMD spans the UV (295–397 nm), while the other two devices have bands in the visible and the near-infrared spectral region (397–580 nm, 580–745 nm); PMDs measure at a high spatial resolution of about $0.36^\circ \times 0.36^\circ$. The cloud amount (CA) of standard GOME pixels at a lower spatial resolution of about 320 km $\times$ 40 km (16 PMDs cover one standard GOME pixel) is then derived by comparing the actual PMD reflectivity measurements (at high spatial resolution) with the cloud-free composite reflectivity maps and performing spatial averaging. See Loyola *et al.* (2007) for more details.

2.2 *Cloud-top height and cloud-top albedo retrieval*

The second algorithm, ROCINN (see also Loyola *et al.* 2007, and references therein) is a neural network algorithm that compares GOME measurements in the O_2 *A*-band with simulated radiances from radiative transfer modelling; the latter are initially computed at high spectral resolution before convolution with the GOME instrument response

function. ROCINN retrieves cloud-top height and cloud-top albedo, and uses the cloud amount originating from the OCRA algorithm as an input parameter. Application of the independent pixel approximation allows us to calculate the total (simulated) reflectance as a weighted sum of contributions from cloudy and cloud-free scenes, where the cloud amount is the desired weighting factor (Kuze and Chance 1994). A data set of simulated reflectances is created for all viewing and solar geometries and geophysical scenarios, and for various combinations of cloud fraction, cloud-top height and cloud-top albedo. The initial ROCINN algorithm was based on transmittance calculations in the O_2 *A*-band only. Currently, we use the Vector Linearized Discrete Ordinate Radiative Transfer (VLIDORT) model (Spurr 2006) in the spectral range 758–772 nm; the simulations now include Rayleigh scattering and polarization since errors induced by using transmittances instead of backscatter reflectances are large, especially for high sun zenith angles. The inversion problem is solved by using neural network techniques. See again Loyola *et al.* (2007) for further details.

Although OCRA and ROCINN are independent algorithms, they are used in tandem in the operational retrieval of GOME cloud properties, in order to achieve the best results. ROCINN requires the cloud amount from OCRA as an input. However, the ROCINN-retrieved cloud-top albedo is then returned as an input to a new OCRA call, in order to refine the cloud coverage retrieval. Thus, the two algorithms are used iteratively, and the iteration stops when changes in cloud amount and the cloud-top albedo are smaller than prescribed thresholds. In practice, only a few iterations are needed for convergence.

The updated version of ROCINN was validated against the same Meteorological satellite (METEOSAT) data record as described in Loyola *et al.* (2007) and Rozanov *et al*. (2006). We now observe a smaller bias of the cloud-top albedo, 0.07 ± 0.09 instead of 0.09 ± 0.10, and at the same time the cloud-top height difference is reduced from -0.63 ± 1.46 km to -0.44 ± 1.26 km.

2.3 *Derived cloud-top pressure and cloud optical thickness*

The cloud-top pressure (CTP) is a straightforward by-product obtained from the cloud-top height provided by ROCINN and a suitable climatological pressure profile. In GOME, we use a single pressure profile for a typical atmosphere (US Standard Atmosphere 1976).

Derivation of cloud optical thickness (COT) is more complex. In order to investigate the relationship between cloud-top albedo and cloud optical thickness, we use the LibRadtran model (Mayer and Kylling 2005) to compute the cloud-top reflectivity (albedo) as a function of COT, surface albedo and illumination and observation angles. Clouds are modelled as scattering layers of water droplets having a gamma droplet size distribution with effective radius 10 μm. Reflectance computations were performed at a wavelength of 760 nm, with a fixed cloud-top height of 4 km. This COT/albedo relationship is shown in figure 1 as a function of the solar zenith angle.

A look-up table of reflectances at 760 nm is computed as a function of cloud-top albedo c_a, surface albedo s_a, solar zenith angle θ_0, satellite zenith angle θ and relative azimuth ϕ. Next, a neural network N is trained with this look-up table, and the inverse problem for cloud optical thickness τ is computed by applying the technique described in Loyola (2006); symbolically we may write

$$\tau = N(c_a, s_a, \theta_0, \theta, \phi). \tag{1}$$

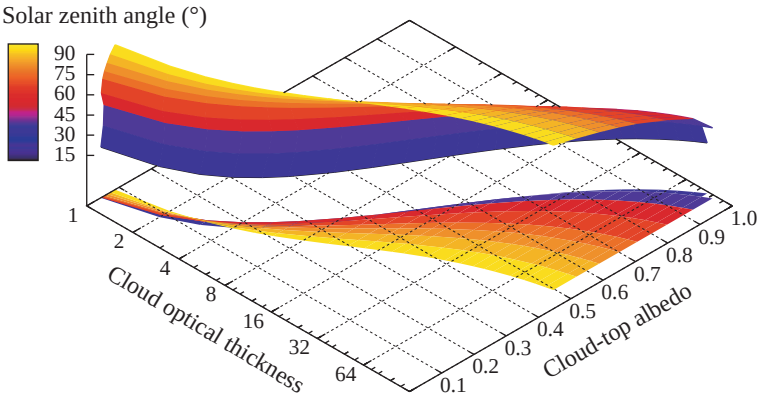

Figure 1. Relationship between cloud-top albedo and cloud optical thickness for different solar zenith angles for a water droplet cloud (mode radius of 10 μm) at a cloud-top height of 4 km, simulated at a wavelength of 760 nm. The cloud optical thickness increases with increasing cloud-top albedo and low solar zenith angles. The increase is less pronounced for high solar zenith angles.

For a given scenario, we use equation (1) to determine cloud optical thickness τ with the cloud-top albedo retrieved by ROCINN as input. We restrict ourselves to values of COT below 100.

2.4 *Computation of monthly mean cloud averages*

With a nominal spatial resolution of 320 km × 40 km, GOME has three forward-scan pixels and one backward-scan pixel covering an orbit swath of 960 km. Global coverage is achieved in 3 days, although the Polar Regions are observed several times a day (see for example figure 2(*a*)). There are more than 30,000 single GOME measurements per day.

In this paper, we determine monthly means of GOME cloud properties on a latitude–longitude grid of resolution 0.33° × 0.33°. The monthly means are computed from the area-weighted average of the daily composites as described in Loyola *et al.*

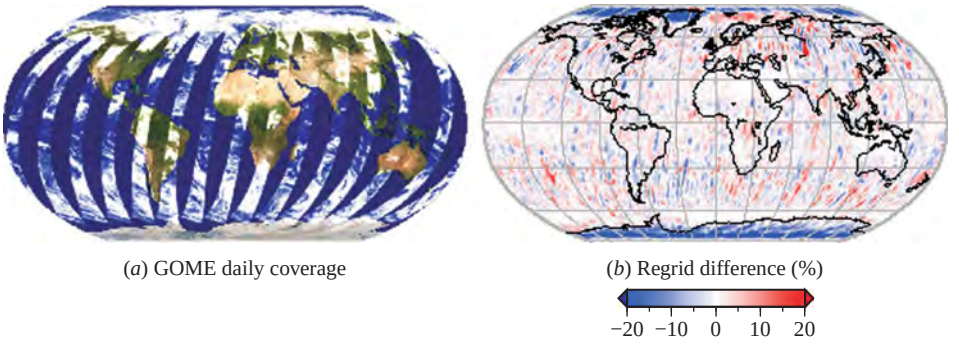

Figure 2. Daily coverage of GOME cloud measurements for 22 May 2002 (*a*). Errors (as percentage differences) induced in the cloud amount monthly mean averages if the area-weighting is omitted (*b*).

(2009). The monthly means are based on somewhere between 7 and 9 million single GOME measurements. Figure 2(*a*) shows the errors induced in the monthly mean cloud amount averages without the use of area-weighting of all the GOME measurements.

3. Global patterns in cloud parameters as derived from GOME observations

This section discusses the variation of cloud parameters as retrieved from GOME observations during the eight-year period from April 1996 to June 2003. As discussed in Aplin (2006), the scale of observation, both in the spatial and temporal domain, should match the scale of processes under observation. GOME footprints are relatively large and the temporal sampling is typically one observation per day, but higher over the polar zones and lower over the tropics. We analysed monthly mean averages and annual averages of cloud parameters in zonal bands. Consequently, the impact of short-term temporal variations of cloud parameters is largely removed. GOME data before April 1996 were not considered because the configuration of GOME (more specifically, the detector integration time and ground pixel size) was not constant during the instrument's one-year commissioning phase after the 20 April 1995 launch. GOME data after June 2003 were excluded because of incomplete global coverage caused by an on-board tape recorder failure at the ERS-2 platform.

3.1 *Inter-annual variation of cloud properties*

In the following we analyse the inter-annual variation of GOME cloud properties (cloud amount, cloud-top pressure and cloud optical thickness) using zonal averages (figure 3). The cloud amount varies strongly with latitude, with largest values occurring in the mid-latitudes (figure 3(*a*)). Over Polar Regions, GOME tends to underestimate the cloud fraction, as it does not have infrared sensors to better discriminate between snow/ice on the ground and low clouds. The northern tropical region appears as the region with the lowest yearly cloud amount. The movement of the cloudless subtropical belts to the north and to the south during the corresponding summer periods is visible in the data but is more pronounced for the Northern Hemisphere. The area of low cloud coverage in the Northern Hemisphere extends to latitudes greater than 30°N, though the equivalent area in the Southern Hemisphere is confined to latitudes less than 30°S. In addition, the winter maximum of cloud amount is more distinct over the Northern Hemisphere.

The annual pattern of the cloud-top pressure (figure 3(*b*)) follows the Intertropical Convergence Zone (ITCZ). Higher clouds with lower cloud-top pressure are present in the Northern Hemisphere during the summer period while the opposite effect is observed during the winter season. The ITCZ is bounded by the trade wind zones, which are often partially covered by low-level marine stratocumulus clouds. These periods of higher cloud-top pressure are visible in the eight years record in the subtropical belts over both hemispheres. There is also a clearly visible seasonal cycle in cloud-top pressure over the southern mid-latitudes. During the winter period, the cloud-top pressure is on average lower than during the summer season. This yearly pattern is less pronounced over the Northern Hemisphere. We believe further that higher clouds (lower cloud-top pressure) in the northern subtropics are linked to the occurrence of the South-East Asian monsoon which is typically present from June to September.

The ITCZ is also visible in the yearly variation of cloud optical thickness (figure 3(*c*)). Clouds in the ITCZ are mainly produced by convection and they are often optically thick.

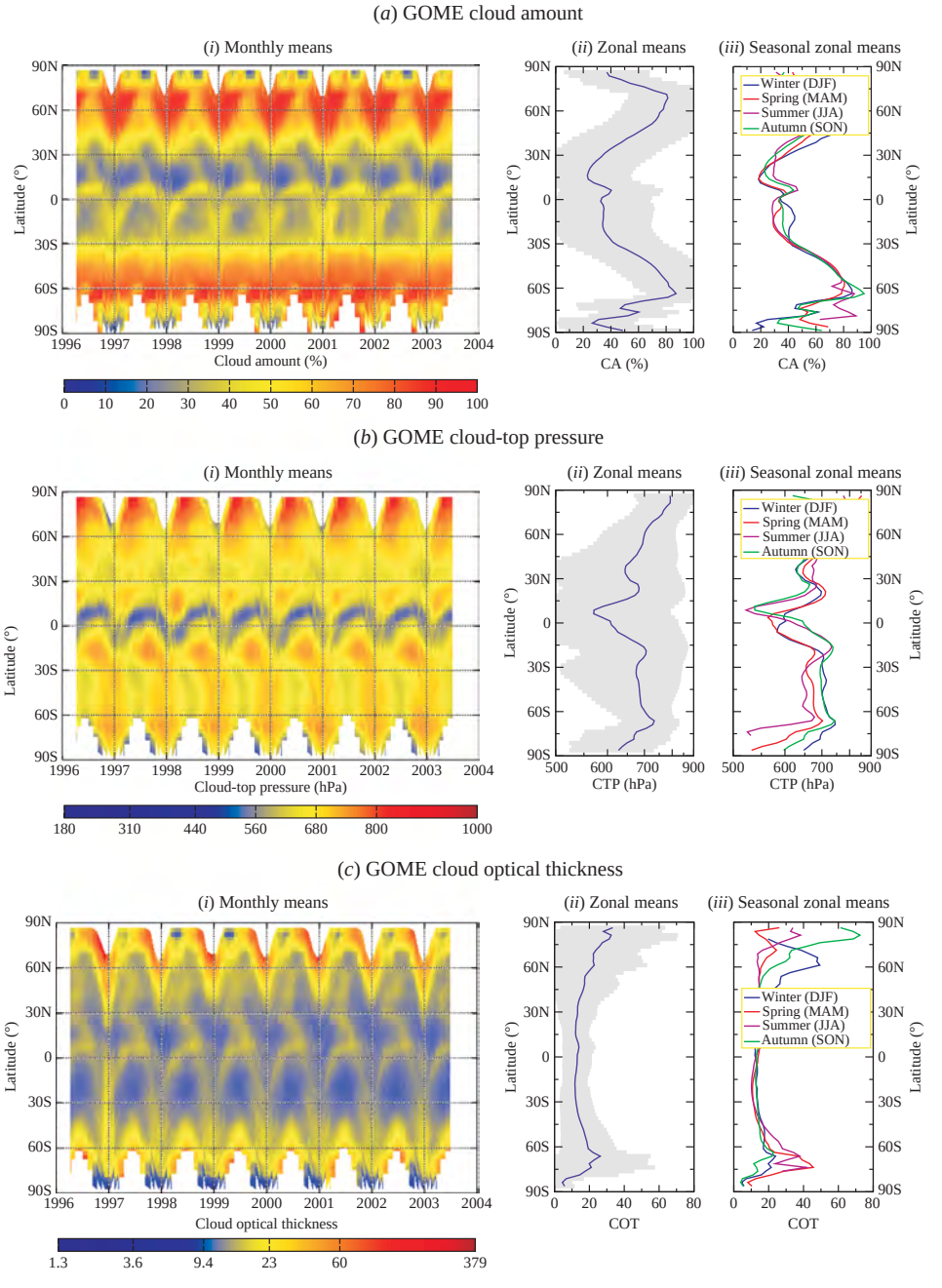

Figure 3. Latitudinal monthly mean (*i*), zonal mean (*ii*) and zonal seasonal mean (*iii*) distributions of the GOME cloud parameters averaged over an 8-year period. (*a*) Cloud amount (CA), (*b*) cloud-top pressure (CTP) and (*c*) cloud optical thickness (COT).

This is reflected in the higher COT values which follow the lower cloud-top pressure values shown in figure 3(*b*). There is also a distinct winter maximum of COT values over both the hemispheres and COT increases from equatorial regions to Polar Regions.

3.2 *Mean cloud properties of zonal bands*

In the following, we analyse GOME cloud properties in zonal bands ranging from northern mid latitudes (35–60°N) to the northern subtropics (15–35°N), the tropical belt (15°N–15°S), the southern subtropics (15–35°S) and the southern mid latitudes (35–60°S). These bands represent the main climate zones (excluding the Polar Regions). Monthly variations of CA, CTP and COT for these bands are displayed in figure 4. The anomalously large cloud amounts at the beginning of 2001 (figure 4(*a*)), which were not evident in figure 3, are artefacts related to problems with the gyroscopes of the ERS-2 satellite, which caused a temporal decrease in the pointing accuracy. In addition, high cloud optical thickness values at the beginning of 1997 are due to technical problems of the GOME detectors (figure 4(*c*)).

Seasonal cycles of all cloud properties are evident for the different regions. Figure 4 shows the cloud properties separately for the Northern and Southern Hemisphere. As expected, there is a 6-month phase shift between cloud properties in the northern and southern tropical belts. This is due to the summer migration of the cloud-rich ITCZ. In contrast with the northern mid latitudes, the cloud amount in the southern mid-latitudes (35–60°S) remains almost stable in time during the entire observation period. The latter region covers the so called 'roaring forties', a latitudinal band between 40°S and 50°S dominated by strong westerly winds associated with troughs along the (often stationary) Rossby wave in the Southern Hemisphere. The cloud amount in this region is therefore relatively high and stable. The cloud amount in the subtropics is lowest (Earth's dry desert zones).

Cloud-top pressure in the northern tropical belt reveals a typical yearly pattern with two minima in June/July and September; this is presumably the combined effect of ITCZ motion and summer monsoon developments. Absolute values of CTP seem to be low for the tropical belt, but one has to take into account the large GOME footprints and the GOME equator crossing at 10:30 ante meridiem (local time) on a sun-synchronous orbit. At this time of the day, convection is typically not well advanced and cloud-top heights will be on average lower than those observed in the afternoon. This is consistent with and indirectly confirmed by the low cloud amount of about 34% in the tropics. In addition, and as already discussed in Loyola *et al.* (2007), GOME often misses optically thin and high cirrus clouds with low cloud-top pressure, leading to an overestimation of the cloud-top pressure.

It is also likely that monsoon systems (in Asia, Africa and America, mainly in the period from June to September) are responsible for a higher mean cloud-top height (lower cloud-top pressure) due to strong convection. The noticeable double (minimum) peak of CTP during the summer period may be related to these regional phenomena. The Earth's monsoon systems occur chiefly in the Northern Hemisphere, and we therefore attribute the southern summer minimum of the cloud-top pressure mainly to the presence of the ITCZ. There is also a seasonal pattern of CTP over the southern tropical belt, but there is no such double minimum peak. The yearly cloud-top pressure variation of the subtropics and the mid-latitude zones is similar but minimum values are typically found later in the winter season of the mid-latitudes (December in the Northern Hemisphere, June/July in the Southern Hemisphere).

The annual variation of cloud-optical thickness is pronounced for both the mid-latitudes and the tropical zones. Over the Northern Hemisphere, this variation is in phase with the cloud amount, in the sense that high cloud coverage corresponds with

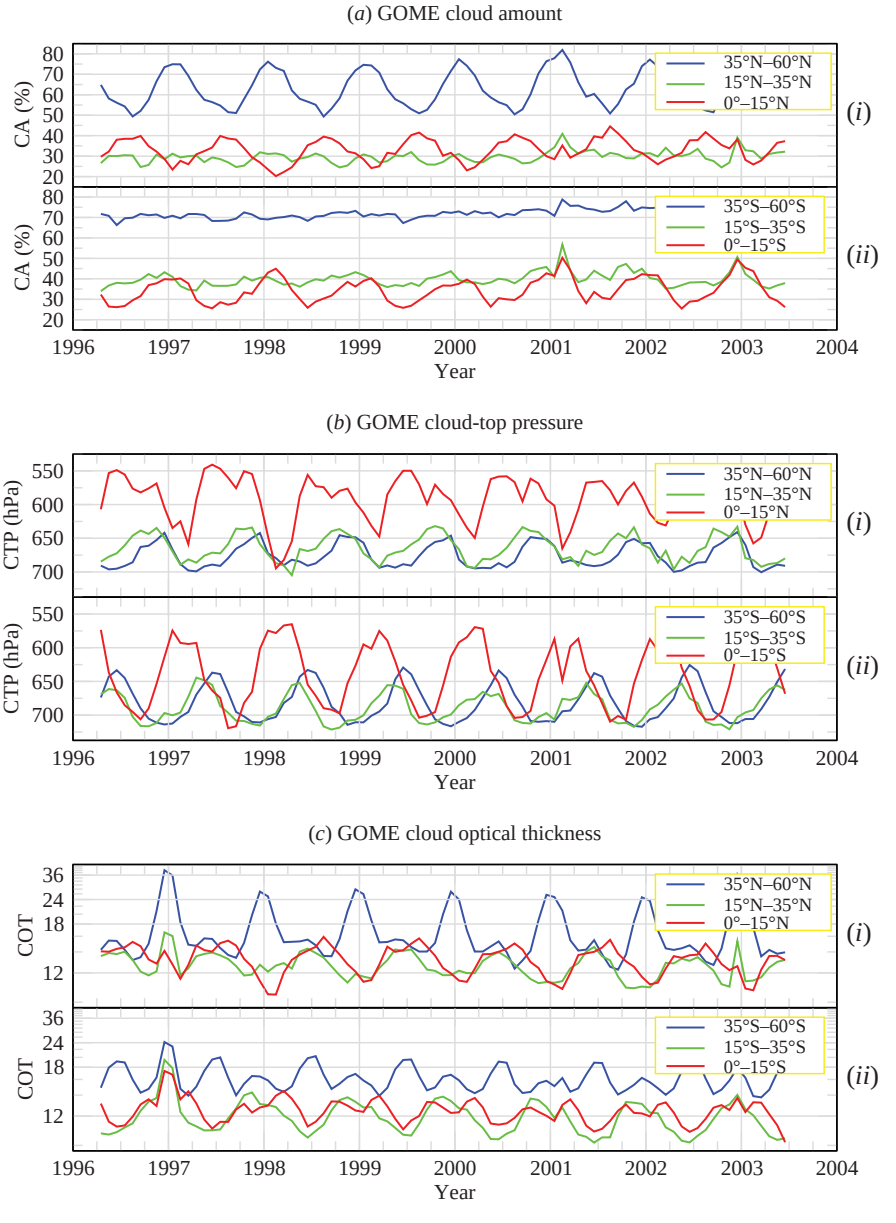

Figure 4. Monthly mean variations of (*a*) GOME cloud amount, (*b*) cloud-top pressure and (*c*) cloud optical thickness in the latitudinal belts 0–15° (red), 15–35° (green), 35–60° (blue). (*i*) Northern Hemisphere graphs; (*ii*) Southern Hemisphere part.

high cloud-optical thickness and vice versa. Again, this effect is less pronounced over the Southern Hemisphere and especially over the mid-latitudes where the variation of the cloud amount is generally low. In the tropics low cloud optical thicknesses during the northern winter season are in line with the maxima of the cloud-top pressure and vice versa. However, the yearly pattern differs for the northern mid-latitudes, where

Table 1. Mean values and standard deviations (one sigma) of cloud properties derived from GOME measurements from April 1996 to June 2003. The number of measurements (in millions) used for the calculation of averages is given in parentheses.

Region	Cloud amount (%)	Cloud-top pressure (hPa)	Cloud optical thickness
35–60°N	62.25 ± 14.75 (99)	677.01 ± 27.78 (94)	16.93 ± 6.80 (94)
15–35°N	29.53 ± 7.49 (58)	664.21 ± 31.53 (47)	12.73 ± 1.59 (47)
0–15°N	33.06 ± 9.12 (41)	589.71 ± 52.76 (35)	13.33 ± 1.66 (35)
0–15°S	34.25 ± 6.59 (41)	640.33 ± 54.99 (35)	12.56 ± 1.32 (35)
15–35°S	39.70 ± 7.25 (60)	689.20 ± 30.45 (55)	12.08 ± 1.67 (55)
35–60°S	71.73 ± 9.09 (105)	685.11 ± 27.58 (102)	16.14 ± 3.47 (102)

high cloud optical thickness during the winter season corresponds with low cloud-top pressure, with a small temporal shift of the minimum cloud-top pressure towards spring. The yearly pattern of COT over the Southern Hemisphere and especially over the mid-latitudes is less variable, as it is for the cloud amount. Absolute COT values are higher over the Northern Hemisphere.

A summary of the regional variation of the cloud properties is given in table 1.

3.3 *Geographical and seasonal distribution of cloud properties*

Global seasonal averages (left panels) and corresponding standard deviations (right panels) of the GOME cloud properties are shown in figures 5–7. As discussed in section 3.1, the mean annual variability of the cloud amount in different latitude bands is well described. We identify a winter maximum of the cloud amount in high latitudes, the minimum throughout the year in the subtropical zones and also regional features such as the increasing cloud amount during the summer monsoon period in South-East Asia and India (figure 5). The standard deviation of mean values is high; this is to be expected, since the natural variability of the cloud amount is large. A small standard deviation during all seasons is therefore found over the Saharan desert and also over higher latitudes where the variability of the cloud coverage is typically lower.

The trade wind zones in the subtropics are often covered by low-level marine stratocumulus clouds. This is reflected in the GOME cloud-top pressure record where these zones are clearly visible (figure 6), mainly over the Atlantic and over the Pacific Ocean. High CTP values are seen over South-East Asia and India during the summer monsoon period that is typically the dominating weather phenomenon there from June to September. Higher CTP values appear also during summer along the Mexican west coast and over the westerly Pacific Ocean where clouds in the ITCZ are responsible for high CTP values.

Seasonal variation of the cloud optical thickness is smooth over large parts of the Earth (figure 7). As for CA and CTP the summer monsoon period in South-East Asia can be identified by larger COT values in that region. The COT values in the trade wind zones are typically smaller than in the ITCZ but differences are not pronounced and remain within the range of the standard deviation of mean values. High values of COT occur in the high latitudes during the winter half year. The effect is more pronounced over the Northern Hemisphere and over the southern polar ocean and along the coastline of Antarctic continent. We believe that this enhancement is an artefact of the COT retrieval – this is known to work less favourably over bright surfaces (Loyola *et al.* 2007).

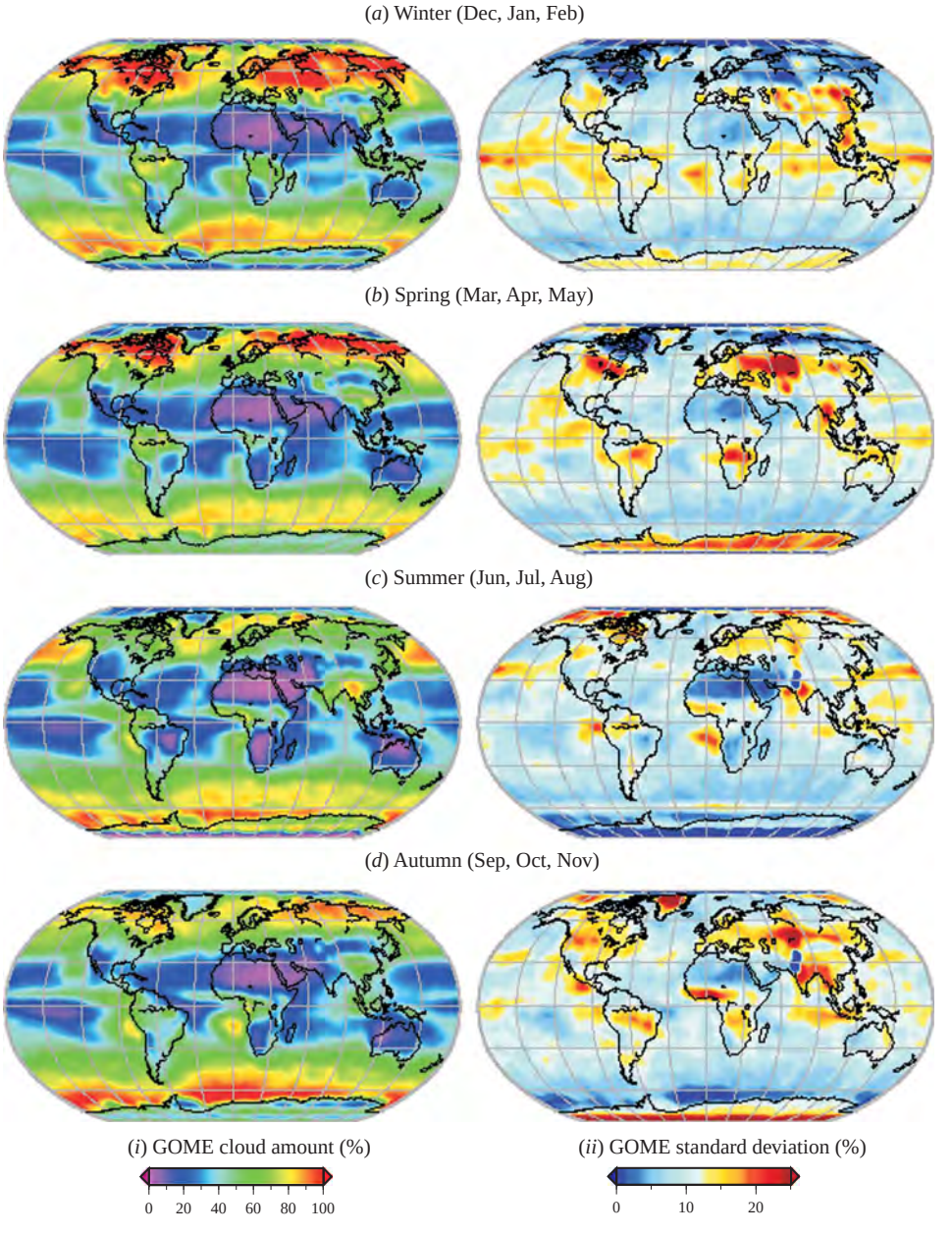

Figure 5. Average seasonal mean variations of GOME cloud amount (*i*) and the corresponding standard deviation (*ii*) from April 1996 to June 2003.

4. Comparisons with ISCCP data

4.1 *Global mean cloud properties*

In this section, we compare global yearly averaged GOME-derived cloud properties with those taken from the combined ISCCP dataset. Analysis of temporally averaged data reduces the noise due to the different spatial and temporal sampling of both the

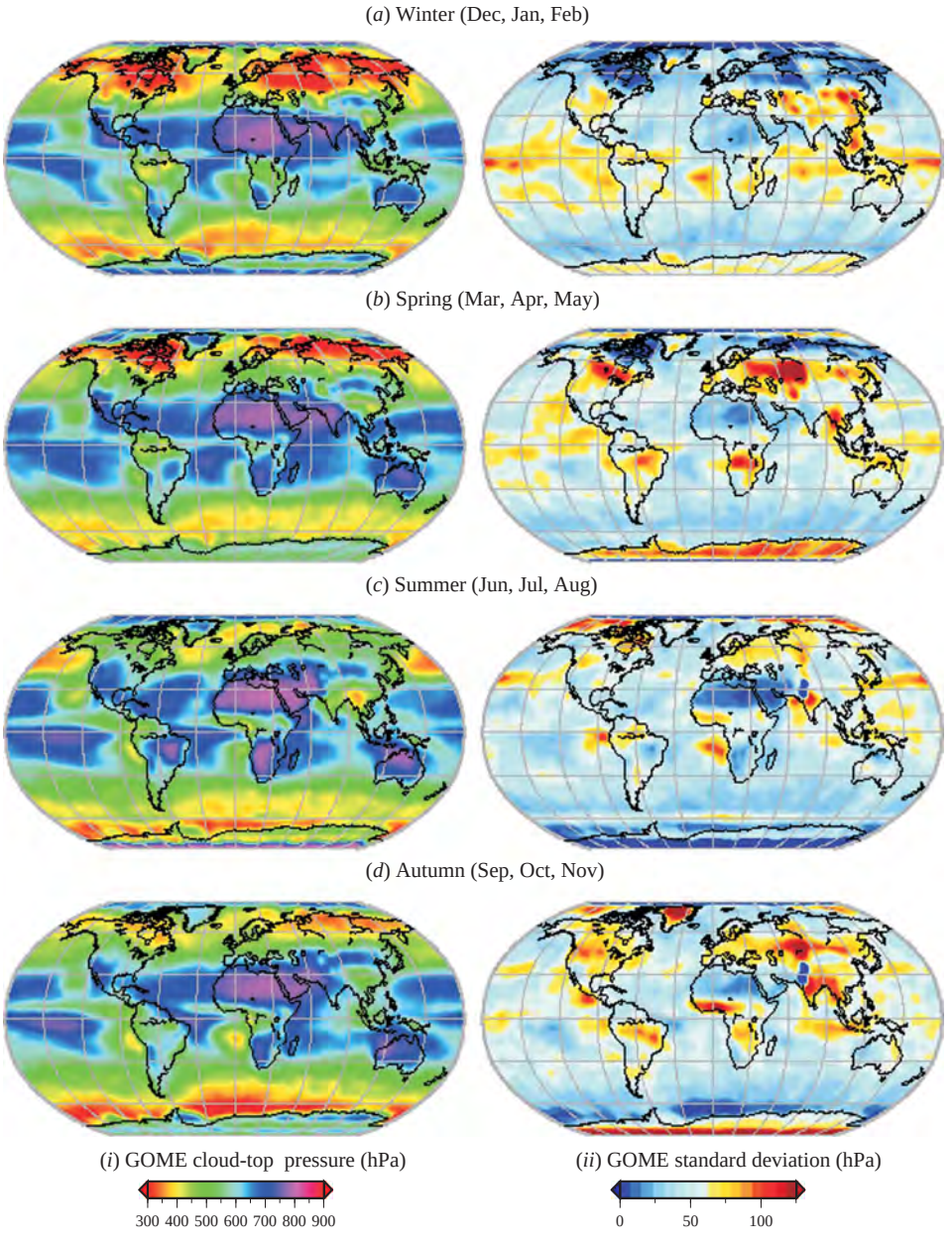

Figure 6. Same as figure 5 but for GOME cloud-top pressure.

GOME and ISCCP data sets. Figure 8(*i*) shows the annual mean distribution of the GOME cloud properties averaged from April 1996 to June 2003. The corresponding ISCCP cloud properties, averaged from the same time period, appear on the right.

Major cloud features seen by GOME and ISCCP match remarkably well. On a global scale, the average GOME cloud amount is about 54%, the average cloud-top pressure is around 680 hPa, and the globally averaged cloud optical thickness is ~17.

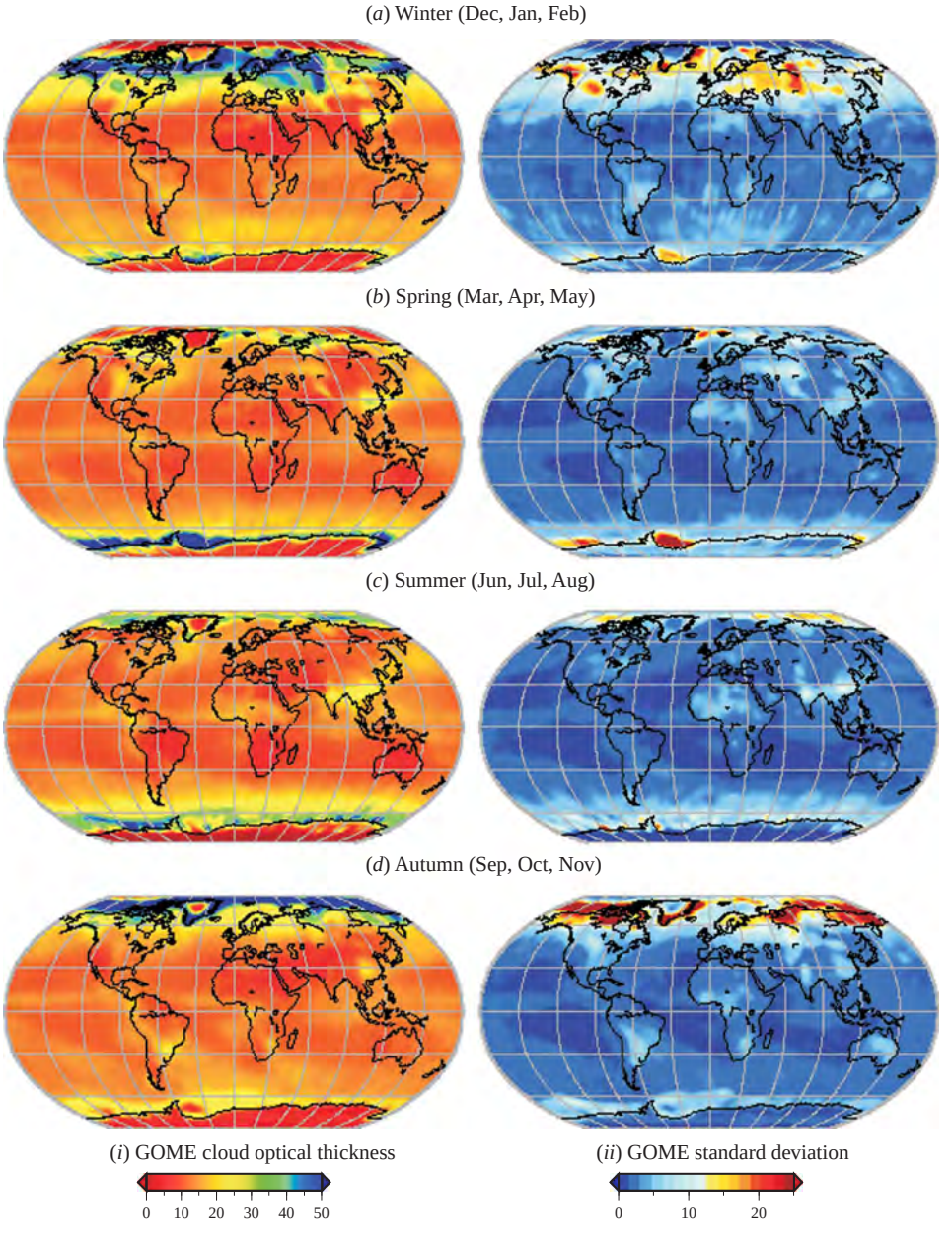

Figure 7. Same as figure 5 but for GOME cloud optical thickness.

The GOME cloud amounts are generally lower than those from ISCCP, largely because GOME misses most optically thin clouds (Loyola *et al.* 2007). However, we note that the two data sets use very different spectral information and retrieval techniques: GOME cloud parameters are retrieved from daytime UV-VIS measurements, whereas ISCCP is based on several day and night visible-infrared (VIS-IR) satellite measurements from a variety of instruments.

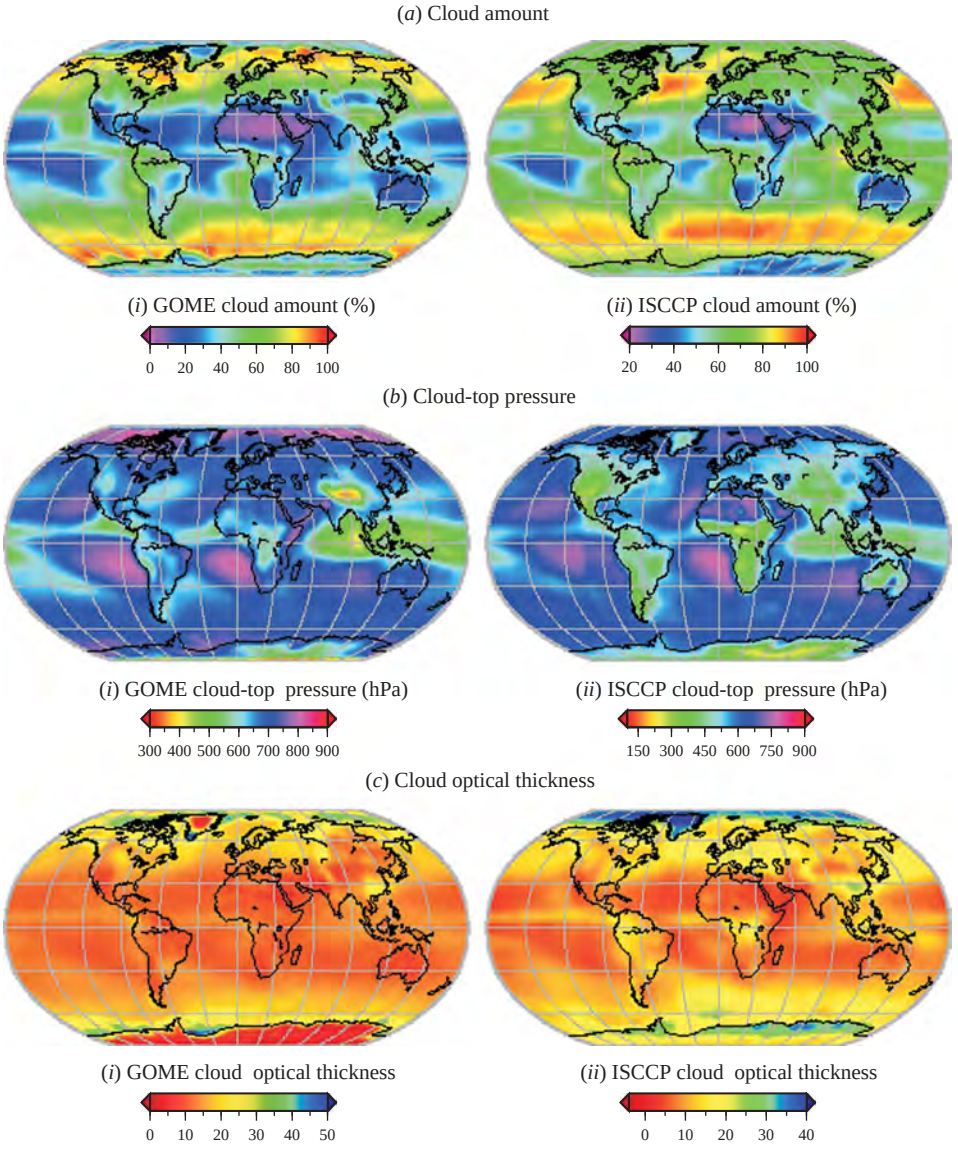

Figure 8. Spatial distribution of 8-year averaged cloud amount (*a*), cloud-top pressure (*b*) and cloud-optical thickness (*c*) as derived from GOME (*i*) and ISCCP (*ii*).

A similar cloud property 'offset' has been observed when comparing ISCCP values with those derived from UV measurements taken by the Ozone Monitoring Instrument (OMI) on board the Aura platform (Vasilkov *et al*. 2008). Data from the HIRS instrument (not shown) reveal a cloud density (number of all observations affected by clouds) of about 75% (Wylie *et al.* 2005). Jin *et al.* (1996) report a larger amount of high-level clouds seen by HIRS than reported by ISCCP (Rossow and Schiffer 1999); this is due to the higher sensitivity of the HIRS instrument to optically thin clouds. These effects result in total cloud coverage about 10–15% higher than that

from ISCCP. In this respect, the GOME cloud amount record is of acceptable quality but with a known offset to other existing data sets.

GOME cloud-top pressure is mostly higher than that from ISCCP. As discussed above, we believe that cirrus clouds with typically low CTP are missing in the GOME record, and this is partially responsible for the observed differences. The mean cloud optical thickness of GOME is slightly lower than the corresponding ISCCP record. The effect is more pronounced over high latitudes (i.e. over bright surfaces), where GOME has problems with cloud detection; see Loyola *et al.* (2007) for a discussion of this limitation.

4.2 *Time series of GOME and ISCCP cloud properties*

Figure 9 shows the GOME and ISCCP mean cloud parameter deviations averaged from 60°N to 60°S and computed from April 1996 to June 2003. The mean GOME cloud amount (figure 9(*a*)) in this latitude band is about 63%, with a positive trend of 0.98%/year over the 8-year record. The mean ISCCP total cloud amount for this band is ∼65%, while there is almost no trend in the cloud coverage. There are however trends in the amount of cloud types, as noted by Zerefos *et al.* (2003) for cirrus clouds, which is presumably due to increasing air traffic. The trend in the GOME series is probably linked to the degradation of the instrument's solar diffuser – this affects the

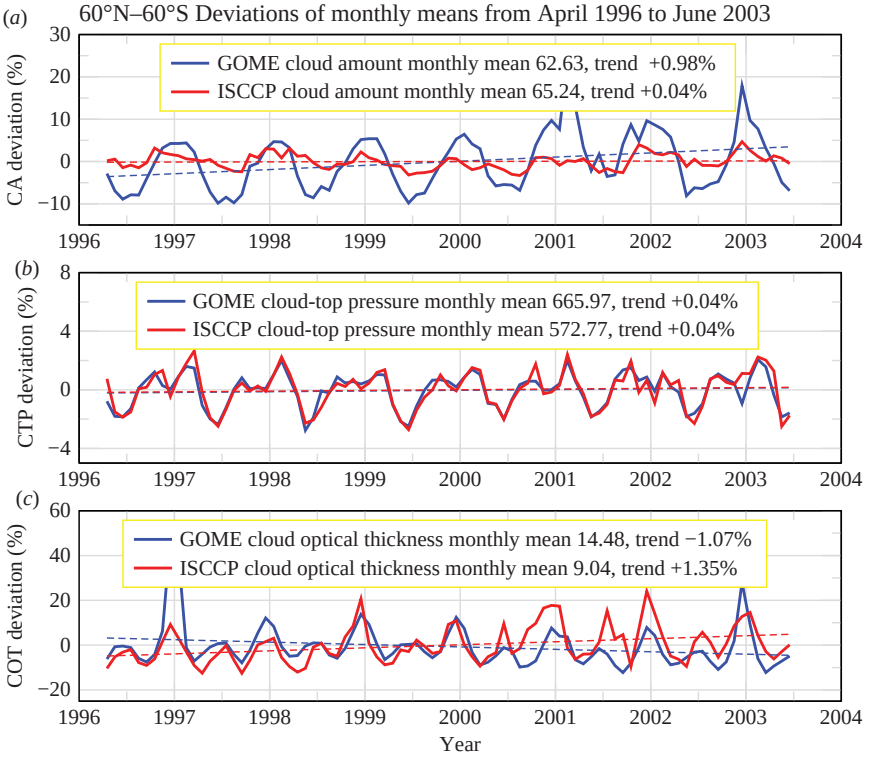

Figure 9. GOME and ISCCP cloud properties deviations (solid lines in blue and red respectively) and trends (dashed lines) averaged over the latitude band 60°N–60°S.

PMD measurements, and the cloud recognition algorithm OCRA is based on reflectivity ratios of PMD backscatter and solar observations. The PMD in the UV spectral range is most subject to degradation of the Sun diffuser. Although a correction for solar diffuser degradation has been incorporated in the operational processing environment, it is not possible to account for the entire degradation effect (Coldewey-Egbers *et al.* 2008) and this may be responsible for small residual trends.

There is no significant trend in the cloud-top pressure (figure 9(*b*)). The mean cloud-top pressure for GOME is about 666 hPa compared with 573 hPa for ISCCP; this result is in line with the known underestimation of the cloud-top height obtained from the oxygen *A*-band measurements (Loyola *et al.* 2007). The mean cloud optical thickness (bottom panel) for GOME is about 14.5 with a negative trend of 1.07%/year. The averaged cloud optical thickness derived from the ISCCP data set is lower (~9) than for GOME while there is a positive trend of 1.35%/year. The negative GOME COT trend is likely due to a feedback effect in the iterative GOME retrieval scheme: as noted in Loyola *et al.* (2007) and Van Roozendael *et al.* (2006), a higher cloud amount is balanced by a lower cloud-top albedo, and this in turn leads to a lower cloud optical thickness. The absolute difference between the mean optical thickness values may be caused by the low sensitivity of GOME with respect to optically thin clouds.

4.3 *Comparison of GOME and ISCCP zonal mean data*

We have analysed zonal mean variations of GOME and ISCCP cloud properties; these are presented in figure 10. Cloud anomalies are calculated as the differences between monthly averages and the overall mean value for the length of the data record (8 years for GOME and ISCCP). Deviations of both GOME and ISCCP from the overall mean are positive in the mid-latitudes but negative in Polar Regions and in the subtropical and tropical regions (figure 10(*a*)). Mean variations of the cloud-top pressure are similar for GOME and ISCCP, although the globally averaged CTP differs by more than 100 hPa (figure 10(*b*)). Zonal variation of the cloud optical thickness is smooth and the variation is close to zero between 60°S and 60°N (figure 10(*c*)). The GOME COT variation is however positive in the northern Polar Regions while it becomes negative over the southern polar area. The corresponding variation in the ISCCP data is smaller, especially towards the South Pole, but it mirrors the GOME data variation over the North Pole area.

4.4 *Cloud parameter frequency distributions*

The global mean frequency distributions of CA, CTP and COT are shown in figure 11. The CA distribution is characterized by two peaks: a primary peak around 30% and a less pronounced secondary peak around 80%. Taking into account the size of the GOME ground pixels (320 km × 40 km) it becomes clear that there is a low probability that an entire GOME pixel is either cloud-free or completely cloud covered. It is therefore more likely that pixels are partially covered, even over large high pressure or low-pressure zones. The cumulative CA histogram is almost linear, indicating an evenly distributed cloud amount.

The CTP frequency distribution has a well-defined peak around 680 hPa; about 80% of the CTP values fall between 560 and 800 hPa. As discussed before, high CTP values occur rarely since high cirrus clouds are mostly missing from the GOME record. In addition, high optically thick clouds do not contribute much to the CTP distribution.

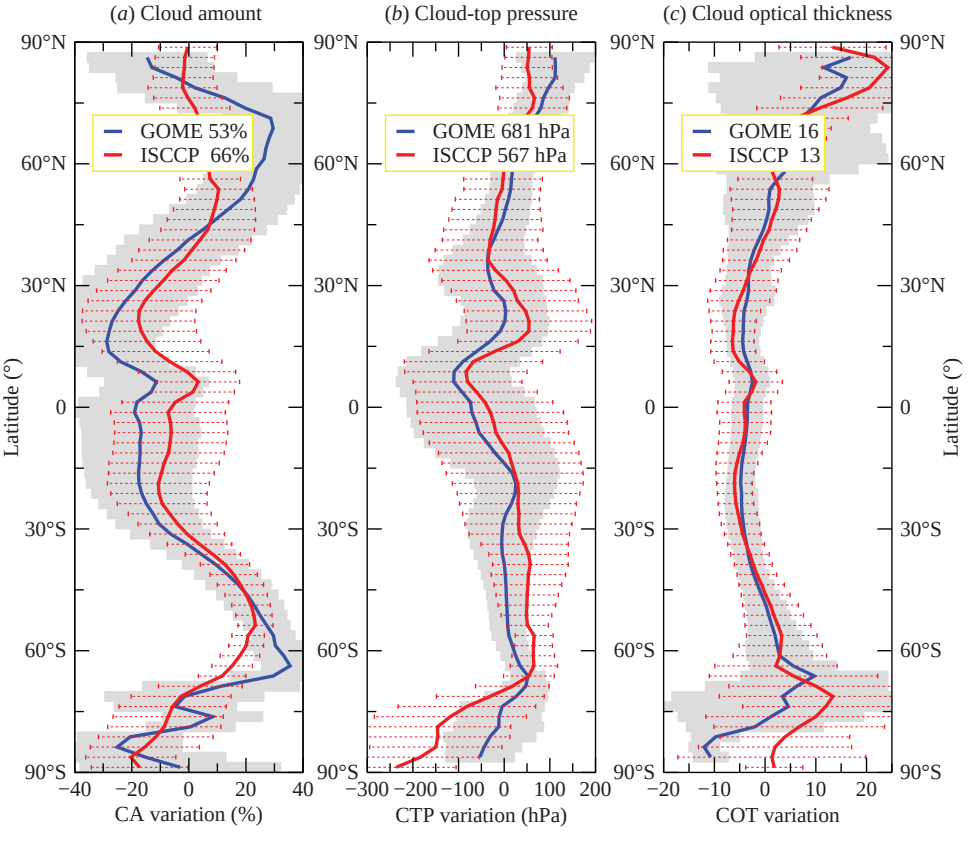

Figure 10. Latitudinal cloud zonal mean variation from April 1996 to June 2003 for GOME in blue, and ISCCP in red. (*a*) Cloud amount anomaly; (*b*) cloud-top pressure anomaly and (*c*) cloud optical thickness anomaly. Global mean values are indicated in the insets. Standard deviations of the GOME (ISCCP) parameters are shown as gray surfaces in the background (dotted red lines in the foreground).

The COT distribution is characterized by a single peak around 10–15; most of the COT values lay between 3.6 and 23. Optically thick clouds (COT $>$ 23) contribute less than 20%, but the contribution of optically thin clouds (COT $<$ 3.6) is even lower ($<$ 5%).

4.5 *Cloud type comparisons*

Although not retrieved from GOME observations, the cloud type can be assigned by application of the ISCCP cloud classification scheme of Stubenrauch *et al.* (1999a). The ISCCP D-series dataset uses classical morphological cloud types as a function of cloud-top pressure and cloud optical thickness (Stubenrauch *et al.* 1999b,c). There are nine cloud types classified according to optical thickness and cloud-top pressure (figure 12).

Using the ISCCP classification scheme, we computed the relative frequency of the nine cloud types for GOME on a monthly basis. We then compared the relative occurrence of GOME and ISCCP cloud types for the 8-year period for which GOME and ISCCP data are both available (figure 13). Stratiform clouds are predominant and comprise more than 75% of all cloud types. Stratocumulus clouds are

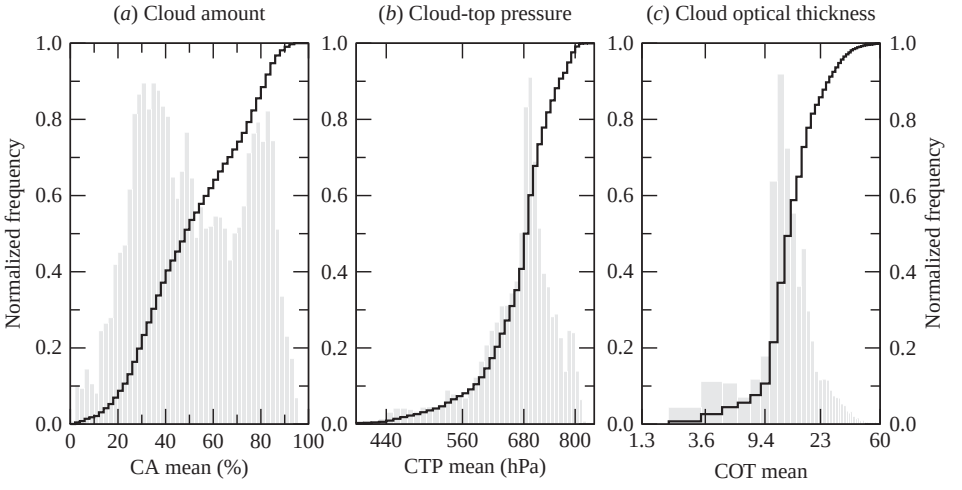

Figure 11. Frequency distribution of (*a*) cloud amount, (*b*) cloud-top pressure and (*c*) cloud optical thickness of GOME global means from April 1996 to June 2003. The normalized histograms are the gray surfaces; the corresponding cumulative histograms are delineated by the black lines.

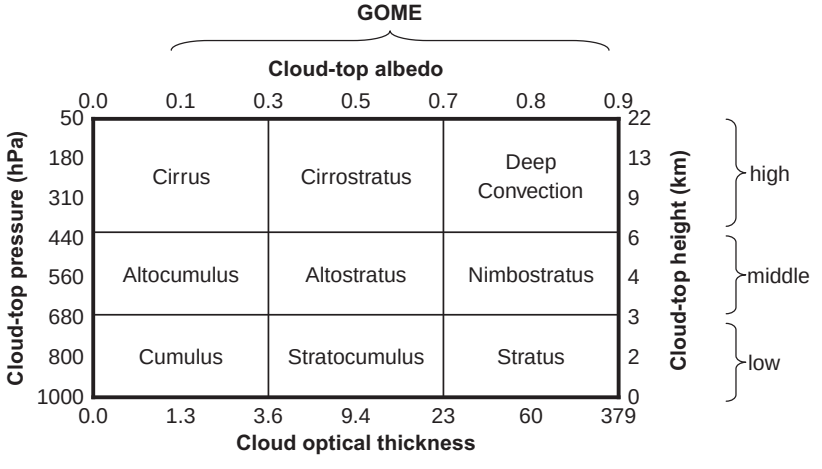

Figure 12. ISCCP D-series cloud types as a function of cloud optical thickness and cloud-top pressure adapted from Stubenrauch (1999c). The approximated range of cloud-top albedo and cloud-top height is given in the top and right axis, respectively. The GOME cloud types do not include optically thin clouds of COT lower than 1.3.

identified in about 41% of all cases; this is a reasonable estimate, since stratocumulus clouds occur frequently over water surfaces covering more than 70% of the Earth's surface. Cirrus clouds seem to be under-represented in both data sets. From Stubenrauch *et al.* (1999a), the global amount of cirrus clouds as derived from satellite instruments is of the order of 10–15%, while we found around 6% for GOME (and a similar value for ISCCP).

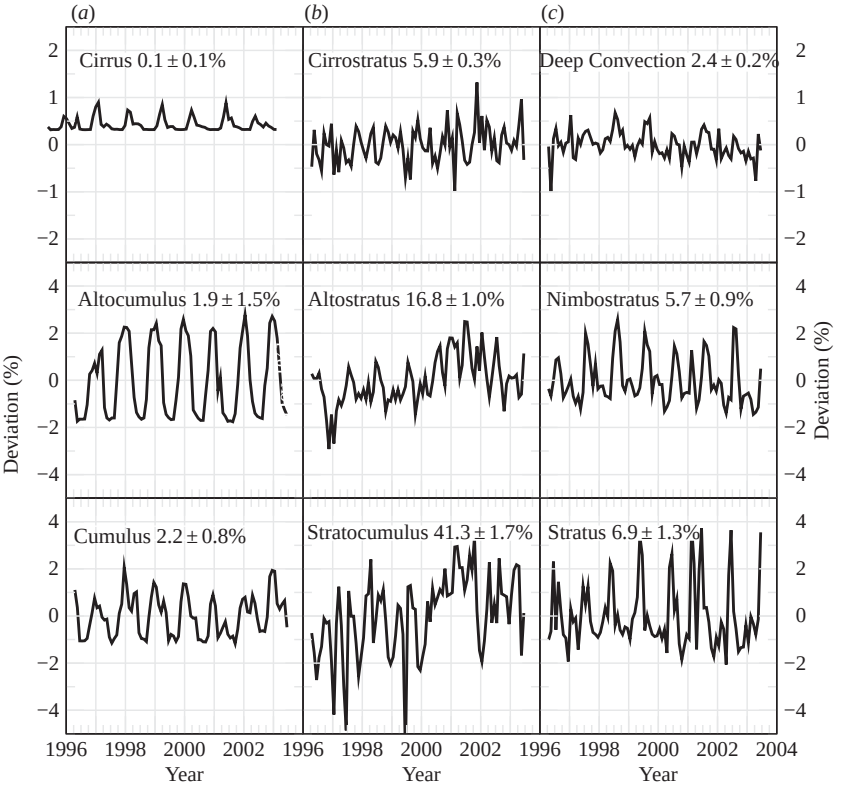

Figure 13. Relative deviation (GOME–ISCCP) between the GOME cloud type distribution and the corresponding ISCCP cloud types using the ISCCP cloud classification method. The relative global occurrence of cloud types and the standard deviation are indicated for each cloud type.

Differences between the GOME and the ISCCP cloud classifications are typically less than 4%. This is a small value, when one takes into account major differences in cloud detection methods and known deficiencies of the GOME instrument for cloud remote sensing (Loyola *et al.* 2007). For some cloud types, and especially for clouds with low optical thickness (less than 5% of all clouds fall into this category), the observed differences follow a yearly pattern which is quite stable throughout the entire period (figure 13(*a*)). For cumuliform clouds and cirrus clouds, maximum (positive) differences appear during the period November to February. Deviations become negative during the period April–August. For most of the stratiform cloud types, we observe maximum positive differences during the Northern Hemisphere summer season, while larger negative differences occur mainly during the corresponding winter season. The exception is with stratocumulus clouds, where deviations from year to year show no clear pattern.

4.6 *Correlated variations of cloud properties*

Two-dimensional histograms of cloud optical thickness versus cloud-top pressure have been used to analyse the correlated variations of cloud properties (Rossow and Schiffer 1999). We have constructed such histograms for the GOME cloud climatology, and the results are discussed in this section.

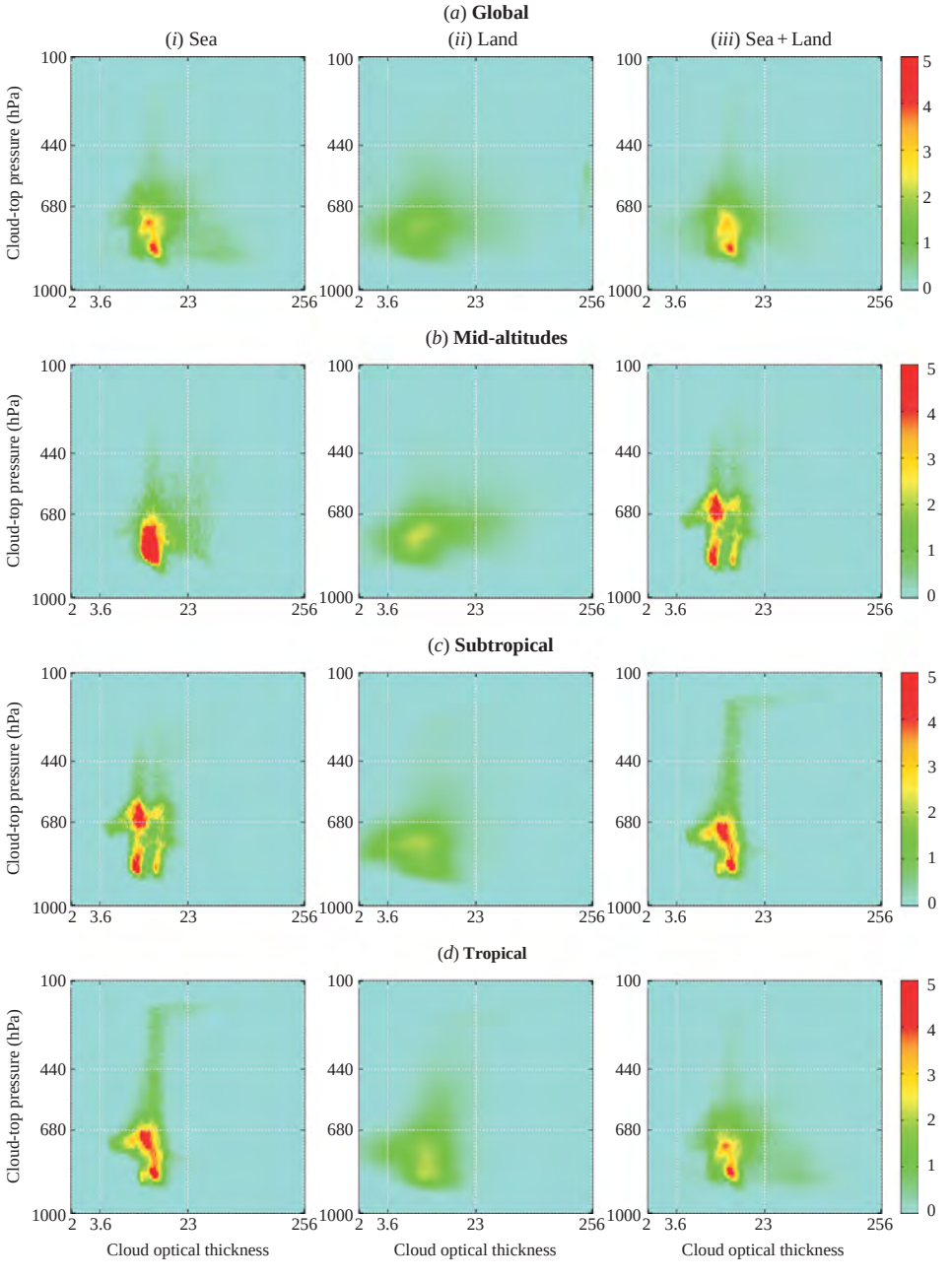

Figure 14. GOME-derived cloud optical thickness and cloud-top pressure variation histograms for different geographical regions: (*a*) global, (*b*) mid-latitudes, (*c*) subtropical and (*d*) tropical. (*i*) Sea areas; (*ii*) land areas; (*iii*) cumulated sea and land histograms. The global distribution is shown in the first row, followed by results of the mid-latitudes, the subtropical and the tropical zone.

Figure 14 illustrates the cloud variation histograms obtained from the averaged GOME data set. Results are shown for sea and land areas and for different geographical regions. On a global scale, we notice a double-peak structure over oceans; this is

not present over land areas. Clouds with similar optical thickness are found in two height regimes which reflect the dominance of maritime stratocumulus clouds (figure 14(*a*)) over water surfaces. Cloud-top height is higher for a narrow band of COT values around 10 over the sea, whereas the corresponding distribution over land is less clear, in the sense that clouds in the lower troposphere there exhibit a large variability of COT values. High clouds are mostly found over water surfaces.

We observe a concentration of low (750–850 hPa) and moderately optically thick clouds (COT $\sim$ 10) in the mid-latitudes. Values concentrate also for optically thicker clouds in the lower troposphere, but higher clouds around 600–700 hPa at lower optical thickness ($\sim$10) contribute to a larger extent (figure 14(*b*)).

Subtropical and tropical regions show large amounts of thin cloud at low and middle levels (figures 14(*c*) and (*d*)). There is also a concentration of optically thin high clouds in these two latitudinal bands. Also, high and optically thick clouds are found in these two regions. Deep convective systems are responsible for this latter contribution.

5. Summary

We have prepared an 8-year record of cloud properties derived from GOME UV-VIS backscatter measurements and we compared the results to the ISCCP D2 data set. We focused on global distributions of cloud amount, cloud-top pressure (height), cloud optical thickness (or its proxy, the cloud-top albedo) and cloud type. We have examined monthly mean averages and standard deviations, and looked at global spatial and seasonal patterns, and frequency distributions. Differences between the GOME and ISCCP records are likely to originate from dissimilar measurement strategies.

The averaged global GOME cloud amount of about 63% is close to the ISCCP global cloud coverage (65%), although the two time series differ in length. Taking further into account the low sensitivity of GOME with respect to optically thin clouds and the large GOME footprints, the consistency of results is remarkably good. In addition, seasonal and geographical distributions of GOME cloud amounts are compatible with current knowledge of global spatiotemporal cloud coverage. It is possible to identify the annual movement of the ITCZ as well as the increasing cloud amount during the Asian monsoon season, the subtropical zones with the Earth's large desert zones and the trade wind zones, and the cloud-rich mid-latitudes (especially in the Southern hemisphere). GOME cloud-top pressures are on average higher (that is, cloud tops are lower) than those from the corresponding ISCCP data. This difference partially originates from the absence of high and optically thin cirrus clouds in the GOME record.

There is also a positive bias between the mean cloud optical thickness of GOME and the corresponding ISCCP value. GOME retrieval is compromised over bright surfaces and the OCRA/ROCINN iterative retrieval of cloud fraction, cloud-top height and cloud-top albedo may be influenced by feedback effects resulting in an overestimation of cloud optical thickness. A comparison of the frequency distribution of cloud types derived from GOME and ISCCP data shows small deviations of a few per cent in all cloud classes. Stratiform clouds dominate the cloud type classification while cirrus clouds seem to be under-represented in both data sets.

We have shown that the current 8-year GOME cloud record is a complementary data set for global cloud studies and for the analysis of long-term climatological effects. However, the time period needs to be extended before trend studies can reveal

statistically significant results. In the near future, we intend to carry out a similar study for SCIAMACHY on-board ENVISAT (in operation since March 2002). Later on, it will be possible to generate cloud records for the GOME-2 instruments on board the MetOp platforms (first satellite launched in October 2006). These newer data sets will extend the GOME cloud record presented here, to provide a comprehensive UV-VIS cloud parameter data record covering a total of 25 years.

Acknowledgements

The authors would like to thank ESA/DLR for providing the GOME level 1 products. The helpful remarks of our reviewers are kindly appreciated.

References

Aplin, P., 2006, On scales and dynamics in observing the environment. *International Journal of Remote Sensing*, **27**, pp. 2123–2140.

Balis, D., Lambert, J.-C., van Roozendael, M., Spurr, R., Loyola, D., Livschitz, Y., Valks, P., Amiridis, V., Gerard, P., Granville, J. and Zehner, C., 2007, Ten years of GOME/ERS-2 total ozone data – The new GOME Data Processor (GDP) Version 4: 2. Ground-based validation and comparisons with TOMS V7/V8. *Journal of Geophysical Research*, **112**, D07307.

Burrows, J.P., Weber, M., Buchwitz, M., Rozanov, V., Ladstätter-Weißenmayer, A., Richter, A., de Beek, R., Hoogen, R., Bramstedt, K., Eichmann, K.-U., Eisinger, M. and Perner, D., 1999, The Global Ozone Monitoring Experiment (GOME): Mission concept and first scientific results. *Journal of Atmospheric Science*, **56**, pp. 151–175.

Chandra, S. and Varotsos, C.A., 1995, Recent trends of the total column ozone – implications for the Mediterranean. *International Journal of Remote Sensing*, **16**, pp. 1765–1769.

Coldewey-Egbers, M., Slijkhuis, S., Aberle, B. and Loyola, D., 2008, Long-term analysis of GOME in-flight calibration parameters and instrument degradation. *Applied Optics*, **47**, pp. 4749–4761.

Evan, A., Heidinger, A. and Vimont, D., 2007, Arguments against a physical long-term trend in global ISCCP cloud amounts. *Geophysical Research Letters*, **34**, L0470.

Grzegorski, M., Wenig, M., Platt, U., Stammes, P., Fournier, N. and Wagner, T., 2006, Technical note: The Heidelberg iterative cloud retrieval utilities (HICRU) and its application to GOME data. *Atmospheric Chemistry and Physics*, **6**, pp. 4461–4476.

Jacobowitz, H., Stowe, L.L., Ohring, G., Heidinger, A., Knapp, K. and Nalli, N.R., 2003, The Advanced Very High Resolution Radiometer Pathfinder Atmosphere (PATMOS) climate dataset: A resource for climate research. *Bulletin of the American Meteorology Society*, **84**, pp. 785–793.

Jin, Y., Rossow, W.B. and Wylie, D.P., 1996, Comparison of the climatologies of high-level clouds from HIRS and the ISCCP. *Journal of Climate*, **9**, pp. 2850–2879.

Karlsson, K.-G., 2003, A 10 year cloud climatology over Scandinavia derived from NOAA Advanced Very High Resolution Radiometer Imagery. *International Journal of Climate*, **23**, pp. 1023–1044.

Karlsson, K.-G., Willen, U., Jones, C. and Wyser, K., 2008, Evaluation of regional cloud climate simulations over Scandinavia using a 10-year NOAA Advanced Very High Resolution Radiometer cloud climatology. *Journal of Geophysical Research*, **113**, D01203.

Koelemeijer, R.B.A., Stammes, P., Hovenier, J.W. and de Haan, J.F., 2001, A fast method for retrieval of cloud parameters using oxygen A-band measurements from the Global Ozone Monitoring Experiment. *Journal of Geophysical Research*, **106**, pp. 3475–3490.

Koelemeijer, R.B.A., Stammes, P., Hovenier, J.W. and de Haan, J.F., 2002, Global distributions of effective cloud fraction and cloud top pressure derived from oxygen A band

spectra measured by the Global Ozone Monitoring Experiment: Comparison to ISCCP data. *Journal of Geophysical Research*, **107**, D4151.

KOKHANOVSKY, A.A., ROZANOV, V.V., ZEGE, E.P., BOVENSMANN, H. and BURROWS, J.P., 2003, A semi-analytical cloud retrieval algorithm using backscattered radiation in 0.4–2.4 μm spectral region. *Journal of Geophysical Research*, **108**, D4008.

KUZE, A. and CHANCE, K.V., 1994, Analysis of cloud-top height and cloud cover-age from satellites using the O2 A and B Bands. *Journal of Geophysical Research*, **99**, pp. 14481–14491.

LINDSTRÖM, J., EKLUNDH, J., HOLST, J. and HOLST, U., 2006, Influence of solar zenith angles on observed trends in the NOAA/NASA 8-km Pathfinder normalized difference vegetation index over the African Sahel. *International Journal of Remote Sensing*, **27**, pp. 1973–1991.

LOYOLA, D., 2006, Applications of neural network methods to the processing of earth observation satellite data. *Neural Networks*, **19**, pp. 168–177.

LOYOLA, D., THOMAS, W., LIVSCHITZ, Y., RUPPERT, T., ALBERT, P. and HOLLMANN, R., 2007, Cloud properties derived from GOME/ERS-2 backscatter data for trace gas retrieval. *IEEE Transactions on Geoscience and Remote Sensing*, **45**, pp. 2747–2758.

LOYOLA, D., COLDEWEY-EGBERS, M., DAMERIS, M., GARNY, H., STENKE, A., VAN ROOZENDAEL, M., LEROT, C., BALIS, D. and KOUKOULI, M., 2009, Global long-term monitoring of the ozone layer – a prerequisite for predictions. *International Journal of Remote Sensing*, **30**, pp. 4295–4318.

MAYER, B. and KYLLING, A., 2005, Technical note: The libRadtran software package for radiative transfer calculations – description and examples of use. *Atmospheric Chemistry and Physics*, **5**, pp. 1855–1877.

MEERKÖTTER, R., KÖNIG, C., BISSOLLI, P., GESELL, G. and MANNSTEIN, H., 2004, A 14-year European Cloud Climatology from NOAA/AVHRR data in comparison to surface observations. *Geophysical Research Letters*, **31**, L15103.

OHRING, G., WIELICKI, B., SPENCER, R., EMERY, B. and DATLA, R., 2005, Satellite instrument calibration for measuring global climate change. *Bulletin of the American Meteorology Society*, **86**, pp. 1303–1313.

ROZANOV, V.V., KOKHANOVSKY, A.A., LOYOLA, D., SIDDANS, R., LATTER, B., STEVENS, A. and BURROWS, J.P., 2006, Intercomparison of cloud top altitudes as derived using GOME and ATSR-2 instruments onboard ERS-2. *Remote Sensing of Environment*, **102**, pp. 186–193.

ROSSOW, W.B. and SCHIFFER, R.A., 1999, Advances in understanding clouds from ISCCP. *Bulletin of the American Meteorology Society*, **80**, pp. 2261–2287.

SCHIFFER, R.A. and ROSSOW, W.B., 1983, The international satellite cloud climatology project ISCCP: The first project of the world climate research programme. *Bulletin of the American Meteorology Society*, **54**, pp. 779–784.

SMITH, P., KALLURI, S., PRINCE, S. and DEFRIES, R., 1997, The NOAA/NASA Pathfinder AVHRR 8-km land data set. *Photogrammetric Engineering and Remote Sensing*, **63**, pp. 12–32.

SPURR, R.J.D., LOYOLA, D., THOMAS, W., BALZER, W., MIKUSCH, E., ABERLE, B., SLIJKHUIS, S., RUPPERT, T., VAN ROOZENDAEL, M., LAMBERT, J-C. and SOEBIJANTA, T., 2005, GOME level 1-to-2 data processor version 3.0: a major upgrade of the GOME/ERS-2 total ozone retrieval algorithm. *Applied Optics*, **44**, pp. 7196–7207.

SPURR, R.J.D., 2006, VLIDORT: A linearized pseudo-spherical vector discrete ordinate radiative transfer code for forward model and retrieval studies in multilayer multiple scattering media. *Journal of Quantitative Spectroscopy and Radiative Transfer*, **102**, pp. 316–342.

STUBENRAUCH, C.J., ROSSOW, W.B., CHÉRUY, F., CHÉDIN, A. and SCOTT, N.A., 1999a, Clouds as seen by satellite sounders (3I) and imagers (ISCCP). Part I: Evaluation of cloud parameters. *Journal of Climate*, **12**, pp. 2189–2213.

STUBENRAUCH, C.J., CHÉDIN, A., ARMANTE, R. and SCOTT, N.A., 1999b, Clouds as seen by satellite sounders (3I) and imagers (ISCCP). Part II: A new approach for cloud parameter determination in the 3I algorithms. *Journal of Climate*, **12**, pp. 2214–2223.

STUBENRAUCH, C.J., ROSSOW, W.B., SCOTT, N.A. and CHÉDIN, A., 1999c, Clouds as seen by satellite sounders (3I) and imagers (ISCCP). Part III: Spatial heterogeneity and radiative effects. *Journal of Climate*, **12**, pp. 3419–3442.

TUINDER, O.N.E., DE WINTER-SORKINA, R. and BUILTJES, P.J.H., 2004, Retrieval methods of effective cloud cover from the GOME instrument: an intercomparison. *Atmospheric Chemistry and Physics*, **4**, pp. 255–273.

US STANDARD ATMOSPHERE, 1976, *US Government Printing Office* (Washington, DC: US Standard Atmosphere).

VAN DIEDENHOVEN, B., HASEKAMP, O.P. and LANDGRAF, J., 2007, Retrieval of cloud parameters from satellite-based reflectance measurements in the ultraviolet and the oxygen A-band. *Journal of Geophysical Research*, **112**, D15208.

VAN ROOZENDAEL, M., LOYOLA, D., SPURR, R., BALIS, D., LAMBERT, J-C., LIVSCHITZ, Y., VALKS, P., RUPPERT, T., KENTER, P., FAYT, C. and ZEHNER, C., 2006, Ten years of GOME / ERS-2 total ozone data: the new GOME Data Processor (GDP) Version 4: I. Algorithm Description. *Journal of Geophysical Research*, **111**, D14311.

VASILKOV, A., JOINER, J., SPURR, R., BHARTIA, P.K., LEVELT, P. and STEPHENS, G., 2008, Evaluation of the OMI cloud pressures derived from rotational raman scattering by comparisons with other satellite data and radiative transfer simulations. *Journal of Geophysical Research*, **113**, D15S19.

WYLIE, D., JACKSON, D.L., MENZEL, W.P. and BATES, J.J., 2005, Trends in global cloud cover in two decades of HIRS observations. *Journal of Climate*, **18**, pp. 3021–3031.

ZEREFOS, C.S., ELEFTHERATOS, K., BALIS, D.S., ZANIS, P., TSELIOUDIS, G. and MELETI, C., 2003, Evidence of impact of aviation on cirrus cloud formation. *Atmospheric Chemistry and Physics*, **3**, pp. 1633–1644.